A dynamically optimized finite difference scheme for large-eddy simulation

Fauconnier D., De Langhe C., Dick E.

In: Journal of Computational and Applied Mathematics, 234, 2080-2088, 2010

A Dynamically Optimized Finite Difference Scheme for Large-Eddy Simulation

D. Fauconnier[1,1], C. De Langhe[1], E. Dick[1]

Department of Flow, Heat and Combustion Mechanics, Ghent University
St. Pietersnieuwstraat 41, B-9000 Ghent, Belgium

Abstract

A low-dispersive *dynamic finite difference scheme* for Large-Eddy Simulation is developed. The dynamic scheme is constructed by combining Taylor series expansions on two different grid resolutions. The scheme is optimized dynamically through the real-time adaption of a dynamic coefficient according to the spectral content of the flow, such that the global dispersion error is minimal. In case of DNS-resolution, the dynamic scheme reduces to the standard Taylor-based finite difference scheme with formal asymptotic order of accuracy. When going to LES-resolution, the dynamic scheme seamlessly adapts to a dispersion-relation preserving scheme. The scheme is tested for Large-Eddy Simulation of Burgers equation. Very good results are obtained.

Key words: Dynamic finite difference approximation, dispersion-relation preserving scheme, Large-Eddy Simulation

1. Introduction

The necessity for numerical quality in Direct Numerical Simulations (DNS) and Large-Eddy Simulations (LES) of turbulent flows, has been recognized by many researchers e.g. Ghosal [1], Kravchenko *et al.* [2] and Chow *et al.* [3]. In a fully resolved DNS, the smallest resolved scales are located far into the dissipation range. Since these scales have only a very small energy-content in comparison with the largest resolved scales in the flow, they are often considered to have a negligible influence on the mean flow statistics. In a Large-Eddy Simulation, however, where only the most important large scale structures are resolved, the smallest resolved scales are part of the inertial subrange and contain relatively more energy than those in the dissipation range. Hence, the smallest resolved scales in Large-Eddy Simulation are not negligible and have a significant influence on the evolution of the LES-flow. The accuracy with which these small scales are described is therefore expected to be important. Moreover, some advanced subgrid modeling techniques such as the dynamic procedure or multiscale modeling strongly rely on the smallest resolved scales in LES, making their accurate resolution even more important. Good numerical quality for an affordable LES is thus vital for accurate flow prediction as it directly influences resolved physics as well as subgrid modeling.
Aside from aliasing errors, which should be prevented by eliminating scales beyond $\kappa_c = \frac{2}{3}\kappa_{max}$, as motivated by Orszag [4], discretization errors are mainly responsible for the loss of numerical accuracy. Since it is highly desirable in LES to maximize the ratio between the physical resolution and the grid resolution κ_c/κ_{max}, in order to lower computational costs, standard second-order central schemes may not be sufficient. Ghosal [1] and Chow *et al.* [3] recommend the filter-to-grid cutoff-ratio to be at most $\frac{\kappa_c}{\kappa_{max}} = \frac{1}{4}$ when using a second-order central scheme. This ensures the magnitude of the discretization errors to be smaller than the magnitude of the modeled force of the subfilter scales, but is prohibitively expensive for most 3D LES computations. Instead, one could apply higher-order discretizations

Email addresses: dieter.fauconnier@ugent.be (D. Fauconnier)
URL: http://www.floheacom.ugent.be (E. Dick)
[1]This research was funded by a PhD grant of the Institute for the Promotion of Innovation through Science and Technology in Flanders (IWT-Vlaanderen).

allowing larger filter-to-grid cutoff-ratios. However, acceptable dispersion errors up to $\kappa_c = \frac{2}{3}\kappa_{max}$, which is the maximum resolution that can be obtained when using the $2/3$-dealiasing procedure, requires at least a standard tenth-order central scheme, or a sixth-order compact Padé scheme, which inevitably leads to increased complexity and computational costs.
In the present work, we develop a *dynamic* low-dispersive finite difference scheme for Large-Eddy Simulation. This scheme, is constructed by combining Taylor series expansions on two different grid resolutions similar to Richardson Extrapolation. A first attempt of this technique has proved successful for obtaining higher accuracy in laminar flows in Fauconnier *et al.* [5, 6]. Further, we show the agreements of the new dynamic scheme with the dispersion-relation preserving scheme of Tam *et al.* [7]. In contrast to their work, the constructed scheme is optimized dynamically during the simulation according to the flow's spectral properties and dispersion errors are minimized through the real-time adaption of a dynamic coefficient. In case of DNS-resolution, the dynamic scheme reduces to the standard finite difference scheme which has an asymptotic order of accuracy. However, going to LES-resolution, the dynamic scheme seamlessly adapts to a dispersion-relation preserving scheme. This could be particularly interesting for transient developing flows, or in case of grid refinement studies with fixed filter width.

2. Construction of the dynamic finite difference scheme

We start by writing the Taylor series expansion for the n^{th}-order derivative, $n = 0, 1, 2, \ldots$, for a k^{th}-order central discretization scheme ($k = 2, 4, 6, \ldots$) on two grid resolutions, characterized by grid spacings $\Delta_1 = \Delta$ and $\Delta_2 = 2\Delta$

$$\overline{\frac{\partial^n u}{\partial x^n}}(x) = \left.\frac{\delta^n \overline{u}}{\delta x^n}\right|^{\Delta} + c_{k,n}\Delta^k \overline{\frac{\partial^{k+n} u}{\partial x^{k+n}}} + \mathscr{O}\left(\Delta^{k+2}\right) \tag{1}$$

$$\overline{\frac{\partial^n u}{\partial x^n}}(x) = \left.\frac{\delta^n \overline{u}}{\delta x^n}\right|^{2\Delta} + c_{k,n}(2\Delta)^k \overline{\frac{\partial^{k+n} u}{\partial x^{k+n}}} + \mathscr{O}\left(\Delta^{k+2}\right) \tag{2}$$

$\overline{u(x)}$ denotes the discrete representation of a continuum physical field $u(x)$ to the discrete grid, while the finite difference approximation of the partial derivative is denoted as $\overline{\frac{\partial}{\partial x}} = \frac{\delta}{\delta x}$. The coefficient $c_{k,n}$ is actually known from the Taylor series expansion. However, suppose that the leading order truncation terms in (1) and (2) are discretized with a minimal order $\mathscr{O}\left(\Delta^2\right)$ and that the Taylor series are truncated to order $\mathscr{O}\left(\Delta^{k+2}\right)$. Then it would be possible to obtain a new value of $c_{k,n}$ by combining (1) and (2). The new $c_{k,n}$ will not necessarily have the same value as the one obtained from identification of the Taylor series, as it is a function of $\overline{u}(x)$, and its derivatives. Moreover, we expect the value of $c_{k,n}$ to be optimized with respect to $\overline{u}(x)$, such that deficiencies of the finite difference approximation, e.g. dispersion errors are minimized. This will be explained later. We first proceed by writing the truncated Taylor series with the discretized leading order truncation terms and we introduce a blending factor f in the second equation

$$\overline{\frac{\partial^n u}{\partial x^n}}(x) = \left.\frac{\delta^n \overline{u}}{\delta x^n}\right|^{\Delta} + c_{k,n}\Delta^k \left.\frac{\delta^{k+n} \overline{u}}{\delta x^{k+n}}\right|^{\Delta} + \mathscr{O}\left(\Delta^k\right) \tag{3}$$

$$\overline{\frac{\partial^n u}{\partial x^n}}(x) = \left.\frac{\delta^n \overline{u}}{\delta x^n}\right|^{2\Delta} + c_{k,n}(2\Delta)^k \left\{ f \left.\frac{\delta^{k+n} \overline{u}}{\delta x^{k+n}}\right|^{2\Delta} + (1-f) \left.\frac{\delta^{k+n} \overline{u}}{\delta x^{k+n}}\right|^{\Delta} \right\} + \mathscr{O}\left((2\Delta)^k\right) \tag{4}$$

To explain the purpose of this blending factor $f \in [0, 1]$ we illustrate the cases $f = 0$ and $f \neq 0$. Remark that, unless $c_{k,n}$ has the exact Taylor value, the order of accuracy in both expressions remains $\mathscr{O}\left(\Delta^k\right)$.

2.1. Asymptotic high-order scheme for $f = 0$

For $f = 0$, the coefficient $c_{k,n}$ can be obtained by subtracting the truncated expressions (4) and (3), leading to

$$\left.\frac{\delta^n \overline{u}}{\delta x^n}\right|^{\Delta} - \left.\frac{\delta^n \overline{u}}{\delta x^n}\right|^{2\Delta} = c_{k,n}\left(2^k - 1\right)\Delta^k \left.\frac{\delta^{k+n} \overline{u}}{\delta x^{k+n}}\right|^{\Delta} \tag{5}$$

Although the left-hand-side and the right-hand-side finite difference approximations do not necessarily have identical stencils, they represent the same derivative. This relation will be used further in this work for simplifications. Substitution of (5) into (3), eliminating $c_{k,n}$, finally leads to the finite difference approximation of order $k+2$

$$\overline{\frac{\partial^n u}{\partial x^n}}(x) = \frac{2^k \left.\frac{\delta^n \overline{u}}{\delta x^n}\right|^{\Delta} - \left.\frac{\delta^n \overline{u}}{\delta x^n}\right|^{2\Delta}}{2^k - 1} + \mathscr{O}\left(\Delta^{k+2}\right) \tag{6}$$

which is the well-known Richardson's Extrapolation formula. It should be emphasized that the same result is obtained by combining (1) and (2) which proves that expression (6) is an approximation with formal asymptotic order of accuracy $k+2$. Since the aim is to construct optimized finite difference schemes with good Fourier characteristics, abandoning the concept of formal asymptotic order of accuracy, obviously f needs to be different from zero.

2.2. Optimized scheme for $f \neq 0$

For the case $f \neq 0$, we proceed in a somewhat different manner as for $f = 0$. Straightforward elimination of $c_{k,n}$ from Taylor series (3) and (4), would lead to a substitution of $c_{k,n}$ with a nonlinear expression. The resulting field for $c_{k,n}$ would be pointwise varying in space, in contrast to the constant value obtained from the Taylor series identification. Here we restrict ourselves to a global grid independent and constant value of $c_{k,n}$, leaving the other possibilities for obtaining $c_{k,n}$ for future work. Therefore, we proceed by subtracting (4) from (3) and obtain

$$\mathscr{E} = \mathscr{L} + c_{k,n}\mathscr{M} = \mathscr{O}\left((2\Delta)^k\right) - \mathscr{O}\left(\Delta^k\right) \tag{7}$$

in which

$$\mathscr{L} = \left.\frac{\delta^n \overline{u}}{\delta x^n}\right|^{\Delta} - \left.\frac{\delta^n \overline{u}}{\delta x^n}\right|^{2\Delta} \tag{8}$$

$$\mathscr{M} = \left(1 - 2^k\right)\Delta^k \left.\frac{\delta^{k+n} \overline{u}}{\delta x^{k+n}}\right|^{\Delta} - 2^k \Delta^k f\left(\left.\frac{\delta^{k+n} \overline{u}}{\delta x^{k+n}}\right|^{2\Delta} - \left.\frac{\delta^{k+n} \overline{u}}{\delta x^{k+n}}\right|^{\Delta}\right) \tag{9}$$

These expressions can be rewritten into a simpler expression on a single grid resolution using the generally valid relation (5), giving

$$\mathscr{L} = c^*_{k,n}\left(2^k - 1\right)\Delta^k \left.\frac{\delta^{k+n} \overline{u}}{\delta x^{k+n}}\right|^{\Delta} \tag{10}$$

$$\mathscr{M} = \left(1 - 2^k\right)\Delta^k \left.\frac{\delta^{k+n} \overline{u}}{\delta x^{k+n}}\right|^{\Delta} - 2^k \Delta^k f\left(c^{**}_{k,n}\left(1 - 2^2\right)\Delta^2 \left.\frac{\delta^{k+n+2} \overline{u}}{\delta x^{k+n+2}}\right|^{\Delta}\right) \tag{11}$$

were $c^*_{k,n}$ and $c^{**}_{k,n}$ are constant coefficients known from Taylor series expansion. For $n = 1$ and $k = 2$ the coefficients are $c^*_{k,n} = -\frac{1}{6}$ and $c^{**}_{k,n} = -\frac{1}{4}$. For $n = 2$ and $k = 2$ the coefficients are $c^*_{k,n} = -\frac{1}{12}$ and $c^{**}_{k,n} = -\frac{1}{6}$. The optimized coefficient can be extracted by least squares minimization of the difference

$$\frac{\partial}{\partial c_{k,n}}\left\langle \mathscr{E}^2 \right\rangle = 0 \tag{12}$$

$\langle \cdot \rangle$ denoting an averaging operator, resulting finally in the dynamic coefficient

$$c^{dyn}_{k,n} = -\frac{\langle \mathscr{L}\mathscr{M} \rangle}{\langle \mathscr{M}\mathscr{M} \rangle} \tag{13}$$

In this work, we restrict ourselves to global uniform averaging over the entire domain. This leads to a constant value coefficient. Substitution of this coefficient into the fine resolution Taylor series leads to the *dynamic finite difference approximation*

$$\overline{\frac{\partial^n u}{\partial x^n}}(x) = \left.\frac{\delta^n \overline{u}}{\delta x^n}\right|^{\Delta} + c^{dyn}_{k,n}\Delta^k \left.\frac{\delta^{k+n} \overline{u}}{\delta x^{k+n}}\right|^{\Delta} \tag{14}$$

The optimal value of f, will be determined in section 2.3. In order to analyze this new dynamic scheme, the Fourier characteristics will be investigated.

2.3. Fourier Analysis

For further investigation of expression (14), we perform a Fourier analysis on the optimized finite difference approximation of the n^{th}-order derivative. In Fourier space, the n^{th} finite difference derivative can be written as

$$\mathscr{F}\left(\frac{\delta^n \overline{u}}{\delta x^n}\right) = (i\kappa'_n)^n \mathscr{F}(\overline{u}) \tag{15}$$

where κ'_n is the modified wavenumber. The ratio of the modified wavenumber to the exact wavenumber represents the error of the discrete derivatives for a single wave with relative wavenumber κ/κ_{max}. The real part of the modified wavenumber κ'_n represents dispersion errors, whereas the imaginary part represents dissipation errors. Remind that the latter are absent in central schemes. The modified wavenumber of a scheme can be obtained by substitution of the discrete wave $\overline{u}(x_{l+r}) = e^{i\kappa(x+r\Delta)}$ into the finite difference approximations. Applying this to the dynamic finite difference approximation for the 1^{st} derivative for basic 2^{nd} order of accuracy ($k = 2$) leads to the modified wavenumber

$$\kappa'_1 = \frac{\left(1 - 2c_1^{dyn}\right)\sin(\kappa\Delta) + c_1^{dyn}\sin(2\kappa\Delta)}{\Delta} \tag{16}$$

and for the 2^{nd} derivative

$$\kappa'^2_2 = \frac{\left(2 - 8c_2^{dyn}\right)(1 - \cos(\kappa\Delta)) + 2c_2^{dyn}(1 - \cos(2\kappa\Delta))}{\Delta^2} \tag{17}$$

in which the dynamic coefficients $c_1^{dyn} = c_{2,1}^{dyn}$ and $c_2^{dyn} = c_{2,2}^{dyn}$ have a constant value. Obviously the 4^{th}-order approximation is recovered if these coefficients equal the theoretical values obtained from Taylor series expansion. However, reminding expression (13), this will generally not be the case, and the value of the coefficients c_1^{dyn} and c_2^{dyn} will depend mainly on the properties of the flow field, its derivatives and the value of f. Since the flow field properties are reflected by the energy spectrum, an attempt is made of analyzing the behaviour of the dynamic coefficients, by transforming the difference definition into Fourier space. Using $\widehat{\cdot}$, to denote the Fourier transform, the difference (7) is given in Fourier space by

$$\widehat{\mathscr{E}}(\kappa) = \widehat{\mathscr{L}} + c_{k,n}\widehat{\mathscr{M}} \tag{18}$$

in which $c_{k,n}$ is the constant dynamic coefficient and

$$\widehat{\mathscr{L}}(\kappa) = c^*_{k,n}\left(2^k - 1\right)\Delta^k\left(i\kappa'_{k+n}\right)^{k+n}\widehat{u} \tag{19}$$

$$\widehat{\mathscr{M}}(\kappa) = \left(1 - 2^k\right)\Delta^k\left(i\kappa'_{k+n}\right)^{k+n}\widehat{u} - 2^k\left(1 - 2^2\right)\Delta^{k+2} f c^{**}_{k,n}\left(i\kappa'_{k+n+2}\right)^{k+n+2}\widehat{u} \tag{20}$$

With this, we can define an error spectrum (* denotes the complex conjugate)

$$E_{\widehat{\mathscr{E}}}(\kappa) = \widehat{\mathscr{E}}\widehat{\mathscr{E}^*} = \widehat{\mathscr{L}}\widehat{\mathscr{L}^*} + c_{k,n}\widehat{\mathscr{M}}\widehat{\mathscr{L}^*} + c_{k,n}\widehat{\mathscr{M}^*}\widehat{\mathscr{L}} + c^2_{k,n}\widehat{\mathscr{M}}\widehat{\mathscr{M}^*} \tag{21}$$

The optimal value for the coefficient $c_{k,n}$ can be found by a least square approximation in Fourier space, defined as

$$\frac{\partial}{\partial c_{k,n}}\int_0^{\frac{\pi}{\Delta}} E_{\widehat{\mathscr{E}}}(\kappa)\, d\kappa \tag{22}$$

Working out this integral expression leads to

$$c_{k,n}^{dyn} = c^*_{k,n}\frac{\displaystyle\int_0^{\frac{\pi}{\Delta}}\left(\kappa'_{k+n}\right)^{k+n}\left[\left(\kappa'_{k+n}\right)^{k+n} + \frac{2^k\left(1-2^2\right)}{1-2^k}\Delta^2 f c^{**}_{k,n}\left(\kappa'_{k+n+2}\right)^{k+n+2}\right]\widehat{u}\widehat{u}^*\, d\kappa}{\displaystyle\int_0^{\frac{\pi}{\Delta}}\left[\left(\kappa'_{k+n}\right)^{k+n} + \frac{2^k\left(1-2^2\right)}{1-2^k}\Delta^2 f c^{**}_{k,n}\left(\kappa'_{k+n+2}\right)^{k+n+2}\right]^2\widehat{u}\widehat{u}^*\, d\kappa} \tag{23}$$

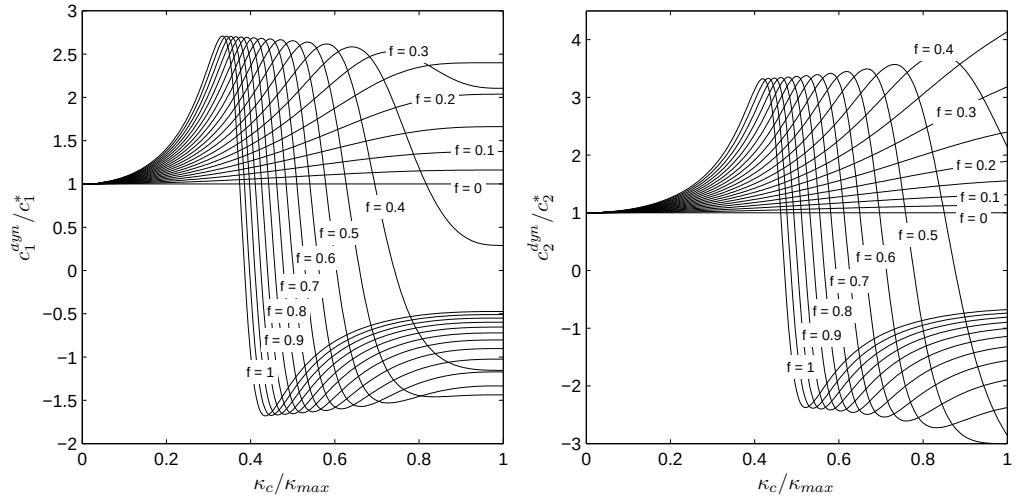

Figure 1: Parametric plot of the dynamic coefficients $c_n^{dyn} = c_{k,n}^{dyn},\ n = 1, 2$ as function of cutoff wavenumber κ_c and the blending factor f.

in which the product $\widehat{uu}^*$ represents the energy spectrum $E_u(\kappa)$ of the physical field $u(x)$. Once the shape of the energy spectrum of the physical field is known or a model spectrum is assumed and a value of the blending factor f is chosen, it is possible to calculate the dynamic coefficient for that spectrum from the integral expression (23). In this work we assume a uniform Heaviside-like spectrum shape

$$E_u(\kappa) \quad = \quad 1 - H(\kappa - \kappa_c) = \begin{cases} 1 & \kappa < \kappa_c \\ 0 & \kappa > \kappa_c \end{cases} \tag{24}$$

with κ_c indicating the highest appearing wavenumber in the signal, or cutoff wavenumber. We note that this shape is chosen for reasons of simplicity, and turbulent spectra will be investigated in future work. The uniform spectrum makes the expression analytically integrable, and the resulting equation describes a surface of the coefficient as function of κ_c and f. This surface is represented as a parametric plot in Figure 1. For $f = 0$ the theoretical values $c_{k,n}^*$ obtained from Taylor series are recovered, regardless the spectral content of the signal which is expressed by the ratio κ_c/κ_{max}. Note also that for smooth signals, with a low ratio κ_c/κ_{max}, the coefficients converge to the theoretical value $c_{k,n}^*$. In case of $f \neq 0$, different profiles for $c_{k,n}^{dyn}$ as function of κ_c/κ_{max} appear. The performance is illustrated in the modified wavenumber plots of Figure 2, where the spectral content of the field is assumed $\frac{\kappa_c}{\kappa_{max}} = \frac{2}{3}$. Clearly, the dynamic finite difference approximation acts as an optimizable k^{th}-order finite difference scheme, in which $c_{k,n}^{dyn}$ is obtained dynamically (for a certain f), according to the flow physics indicated by κ_c. As can be seen from the figures, different values of f lead to different behavior of the dynamic scheme and different accuracy. It is clear that if the ratio $0 \leq c_{k,n}^{dyn}/c_{k,n}^* < 1$, the schemes Fourier characteristic will lie between that of the k^{th}-order and $(k+2)^{nd}$-order standard scheme, and does not result into the desired behavior. Moreover, if $c_{k,n}^{dyn}$ has an opposite sign in comparison with its Taylor value, i.e. $c_{k,n}^{dyn}/c_{k,n}^* < 0$, poor Fourier characteristics are observed that lie below that of the k^{th}-order scheme. Hence, the f-values should be chosen such that $c_{k,n}^{dyn}/c_{k,n}^* \geq 1$ for all values of κ_c/κ_{max}. Moreover, since $c_{k,n}^{dyn}$ acts like a sensor for the wavenumber content in the field $\overline{u}(x)$, it should be a monotonic function of κ_c/κ_{max} such that each value of $c_{k,n}^{dyn}$ corresponds to a unique value of κ_c/κ_{max}. Hence, the blending factor f should be determined such that monotonicity of $c_{k,n}^{dyn}$ in the wavenumber range $0 \rightarrow \kappa_c$ is guaranteed. It can be understood from the modified wavenumber plots (Figure 2) that for a certain ratio of κ_c/κ_{max}, an optimal value of f exists that satisfies both previous conditions and for which the corresponding value of $c_{k,n}^{dyn}$ leads to an optimal finite difference scheme.

Clearly, the dynamic finite difference approximation is an optimized 2^{nd}-order finite difference scheme with better performance at the small scales, in which $c_{k,n}^{dyn}$ is obtained dynamically (for a certain value of f), according to the flow's spectral properties, related to κ_c. These findings display a large agreement with the work of Tam *et al.* [7] in the field of computational aeroacoustics, who introduced an explicit dispersion-relation preserving finite difference scheme (DRP

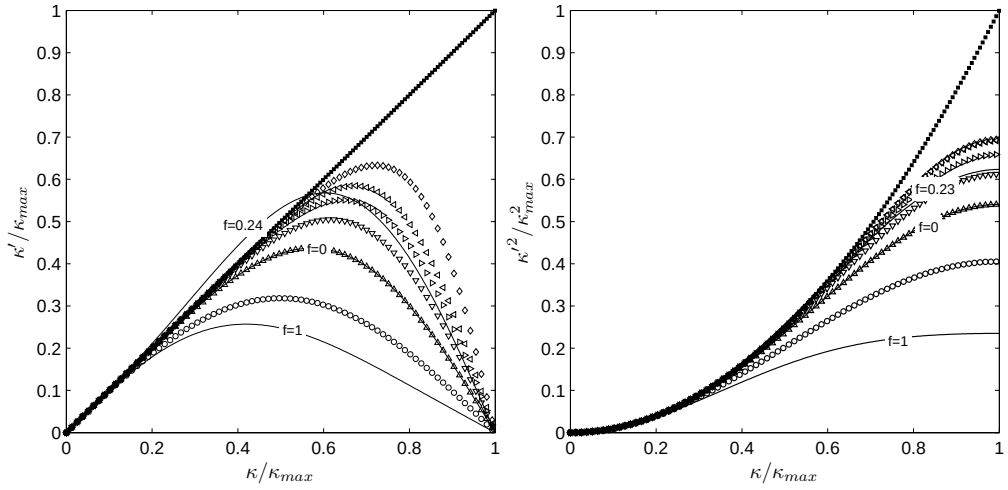

Figure 2: Modified wavenumber for $\frac{\delta u}{\delta x}$ (left) and $\frac{\delta^2 u}{\delta x^2}$ (right). (■) *spectral; (∘) 2^{nd}-order central; (△) 4^{th}-order central; (▽) 6^{th}-order central; (▷) 8^{th}-order central; (◁) 10^{th}-order central; (⋄) 6^{th}-order tridiagonal Padé; (—) 2^{nd}-order dynamic scheme.*

scheme) for accurate simulation of propagating waves, where such highly non-dispersive and non-dissipative schemes are required. These DRP schemes are constructed by a priori minimization of the dispersion error, represented by the modified wavenumber in the wavenumber range $\kappa = 0 \rightarrow \frac{\pi}{\Delta}$. Such a scheme can be constructed by finding the optimal $c_{k,n}$ in (16) and (17). However, in contrast to the DRP schemes with fixed Fourier characteristics, the *dynamic finite difference scheme* optimizes its coefficient according to the flow physics, leading to adaptive Fourier characteristics. This way, the scheme varies between the asymptotic 4^{th}-order finite difference approximation and DRP-like 2^{nd}-order finite difference scheme, depending on the spectral content represented on the grid. As can be seen from the figures, different values of f lead to different behavior of the dynamic scheme and different accuracy. As mentioned before, f-values for which the optimized coefficient $c_{k,n}^{dyn}$ is not monotonically decreasing as function of the spectral content (e.g. $f = 1$), lead to poor performance of the schemes. The figures indicates that a value of f can be found for which the scheme is optimal for a given spectral content κ_c.
Traditionally, the optimization is done by minimizing the least squares error of the modified wavenumber and the real wavenumber [7]. Assume the following error definition

$$\widehat{\mathscr{E}}(\kappa) \quad = \quad i^n \left(\kappa^n - \kappa'(\kappa, f)^n\right) \Delta^n \widehat{u} \tag{25}$$

which represents the error between the exact n^{th} derivative and its finite difference approximation in Fourier space. Now we define the error spectrum as

$$E_{\widehat{\mathscr{E}}}(\kappa) \quad = \quad \widehat{\mathscr{E}}\widehat{\mathscr{E}}^* = \left(\kappa^n - \kappa'(\kappa, f)^n\right)^2 \Delta^{2n} \widehat{u}\widehat{u}^* \tag{26}$$

The product $\widehat{u}\widehat{u}^*$ represents the energy spectrum $E_u(\kappa)$ of the physical field $u(x)$. The optimal value for the blending factor f can be found by searching the minimum of the integral over all wave components or

$$\frac{\partial}{\partial f} \int_0^{\frac{\pi}{\Delta}} \left(\kappa^n - \kappa'(\kappa, f)^n\right)^2 E_u(\kappa)\, d\kappa = 0 \tag{27}$$

Adopting a uniform spectrum $E_u(\kappa)$ (24), the integral can be calculated analytically leading to a rather complicated expression for the optimal blending factor as function of the highest appearing wavenumber κ_c, $f_{opt} = f(\kappa_c)$. Most dispersive errors exist in the range $\frac{2}{3}\kappa_{max} < \kappa_c < \kappa_{max}$. However, it is preferable that this wavenumber range is omitted in the optimization. Minimizing the errors in this range would be meaningless, since in a good simulation, this region should be eliminated because of aliasing errors. Choosing $\kappa_c = \frac{2}{3}\kappa_{max}$, the optimal values of the blending factors for the 1^{st} and 2^{nd} derivative are $f_1^{opt} = 0.2403$ and $f_2^{opt} = 0.2315$. Using the same methods, an optimized 2^{nd}-order DRP

scheme can be constructed in which the optimal *static* coefficients in equations (16) and (17) are $c_1^{dyn} = -0.3344$ and $c_2^{dyn} = -0.1346$, identical to $c_1\left(f_1^{opt}\right)$ and $c_2\left(f_2^{opt}\right)$ for the uniform spectrum at $\kappa_c = \frac{2}{3}\kappa_{max}$.

3. Numerical test case

For a first evaluation of the developed schemes for Large-Eddy Simulation, it may be more useful to consider a simpler equivalent problem than LES of three-dimensional Navier-Stokes turbulence. Following the work of Das *et al.* [8], we select the one-dimensional viscous Burgers' equation. Similar to the Navier-Stokes equations, the Burgers' equation contains a quadratic nonlinear term and it exhibits an inertial range in the energy spectrum as in real turbulence. Although the small-scale dynamics of the Burgers' turbulence and real turbulence are substantially different since the small scales represent shock waves with thickness in the order of the viscous scale, this is of minor importance for the evaluation of numerical schemes. The Burgers' equation is given in its non-dimensional form by

$$\frac{\partial u}{\partial t} + \frac{1}{2}\frac{\partial u^2}{\partial x} = \frac{1}{\mathrm{Re}}\frac{\partial^2 u}{\partial x^2}, \quad \mathrm{Re} = \frac{1}{\nu} \tag{28}$$

which we subject to periodic boundary conditions $u(x,t) = u(x+2\pi,t)$ in the periodic domain $0 \leq x \leq 2\pi$. The initial condition at $t = 0$ imposes the sinusoidal velocity profile $u(x,0) = \sin(x)$, representing a single wave mode. The initial values of the kinetic energy and dissipation rate are $k(t=0) = 1/4$ and $\varepsilon(t=0) = 1/\mathrm{Re}$. For $t > 0$, the single wave evolves in time and finally runs into a stationary shock at $x = \pi$, which is damped by viscous forces. As mentioned before, the corresponding shock wave energy spectrum exhibits an inertial range κ^{-2}, through which energy is transferred from the large scales to the small scales, and finally dissipated in the dissipation range by the viscosity. The Reynolds number is set to $\mathrm{Re} = 1/\nu = 500$.

3.1. Direct Numerical Simulation of Burgers' equation

First, a reference solution for the Burgers' system is generated from a Direct Numerical Simulation. A uniform grid is adopted with $n_x = 8192$ nodes, for which the grid cutoff wavenumber $\kappa_{max} = \frac{\pi}{\Delta_{DNS}} = 4096$, such that all scales, including all viscous scales in the dissipation range, are very well resolved. The simulation is done using a pseudo-spectral code, avoiding numerical discretization errors. Dealiasing is not required since all scales are well resolved and no aliasing errors can appear. The standard 4-stage low-storage Runge-Kutta time stepping with coefficients $\left[\frac{1}{4}, \frac{1}{3}, \frac{1}{2}, 1\right]$ is adopted. The time step is set to $\Delta t = 1e^{-5}$ and the shock wave is followed until $t = 10$.

3.2. Large-Eddy Simulation of the Burgers' equation

The goal of LES is to reproduce the dynamics of the filtered DNS-solution, by resolving only the high-energetic large scale features (low wavenumbers) in the flow, corresponding to ideally 80% of the total kinetic energy, while neglecting the low energetic small scales (high wavenumbers). This philosophy requires the definition of an appropriate spatial filter. In this work, a sharp spectral Fourier filter is used. Applying a sharp Fourier filter with cutoff $\kappa_c = \frac{\pi}{\Delta_f}$ to the continuous equation (28), denoting $\widetilde{\cdot}$ as the filtered quantity, gives

$$\frac{\partial \widetilde{u}}{\partial t} + \frac{1}{2}\frac{\partial \widetilde{\widetilde{u}\,\widetilde{u}}}{\partial x} = \frac{1}{\mathrm{Re}}\frac{\partial^2 \widetilde{u}}{\partial x^2} - \frac{1}{2}\frac{\partial \tau}{\partial x} \tag{29}$$

in which the subgrid stress is $\tau = \widetilde{uu} - \widetilde{\widetilde{u}\,\widetilde{u}}$. In this equation, the nonlinear term is explicitly filtered in order to avoid aliasing. Now the equation can be discretized from continuum space $\mathbb{R}$ to the discrete space with grid resolution $\kappa_{max} = \frac{\pi}{\Delta}$, leading to

$$\frac{\delta \widetilde{u}}{\delta t} + \frac{1}{3}\underline{\widetilde{u}}\frac{\widetilde{\delta u}}{\delta x} + \frac{1}{3}\frac{\widetilde{\delta \widetilde{u}\,\widetilde{u}}}{\delta x} = \frac{1}{\mathrm{Re}}\frac{\delta^2 \widetilde{u}}{\delta x^2} - \frac{1}{2}\frac{\delta \tau}{\delta x} \tag{30}$$

Remark that the sampled field is denoted as $\overline{\widetilde{u}} = \widetilde{u}$ in order to avoid overload of notation and that the nonlinear term is discretized in the skew-symmetric form to guarantee the discrete conservation of kinetic energy [9]. Following the work of Orszag [4] we define $\kappa_c = \frac{2}{3}\kappa_{max}$. Since equations (29) and (30) are unclosed, an appropriate subgrid

scale model is needed to close the equations. In this work, we use a *perfect subgrid scale model*, in which the exact subgrid stresses are extracted at each Runge-Kutta step from a simultaneously running Direct Numerical Simulation. This results in a perfect LES in which the filtered DNS results are recovered exactly. The Large-Eddy Simulation of the Burgers' equation is done on a uniform mesh with $n_x = 256$ nodes, for which the grid cutoff wavenumber is $\kappa_{max} = \frac{\pi}{\Delta} = 128$ and the physical cutoff wavenumber defined by the filter $\kappa_c = \frac{2}{3}\kappa_{max} = 85$. Different central finite difference discretizations will be investigated.

4. Numerical Results

The numerical errors of the different finite difference schemes on the solution of a Large-Eddy Simulation of Burgers' equation are investigated after defining an appropriate error evaluation.

4.1. Quantification of numerical errors

To quantify numerical errors due to finite difference approximations, we use the error decomposition as defined by Vreman *et al.* [10] and Meyers *et al.* [11], which tries to separate modeling errors from numerical errors. Consider a reference DNS in which the smallest viscous scale is represented by κ_η, and assume a specific flow variable of interest ϕ. The total error in ϕ for a Large-Eddy Simulation with grid resolution $\kappa_{max} = \frac{\pi}{\Delta}$ and filter resolution $\kappa_c = \frac{\pi}{\Delta_f}$ is then defined as

$$\varepsilon_{\phi,total}\left(\kappa_c, \kappa_{max}\right) = \widetilde{\phi_s\left(\kappa_\eta, \frac{3}{2}\kappa_\eta\right)} - \widetilde{\phi}_{fd}\left(\kappa_c, \kappa_{max}\right) \tag{31}$$

The error is explicitly defined as function of the LES filter resolution and grid resolution and $\widetilde{\phi_s\left(\kappa_\eta, \frac{3}{2}\kappa_\eta\right)}$ represents the filtered *spectral* DNS solution, while $\widetilde{\phi}_{fd}\left(\kappa_c, \kappa_{max}\right)$ represents the *finite difference* LES solution with filter cutoff κ_c on an LES grid with maximum wavenumber κ_{max}. The total error consists of contributions of numerical errors and modeling errors and is decomposed as

$$\varepsilon_{\phi,model}\left(\kappa_c, \kappa_\eta\right) = \widetilde{\phi_s\left(\kappa_\eta, \frac{3}{2}\kappa_\eta\right)} - \widetilde{\phi}_s\left(\kappa_c, \kappa_{max}\right) \tag{32}$$

$$\varepsilon_{\phi,num}\left(\kappa_c, \kappa_{max}\right) = \widetilde{\phi}_s\left(\kappa_c, \kappa_{max}\right) - \widetilde{\phi}_{fd}\left(\kappa_c, \kappa_{max}\right) \tag{33}$$

$\widetilde{\phi}_s\left(\kappa_c, \kappa_\eta\right)$ represents the *spectral* LES-solution with filter cutoff wavenumber κ_c and grid cutoff wavenumber κ_{max} corresponding to the LES grid, and would be equivalent with the *finite difference* LES-solution on an infinitely fine grid. The modeling error $\varepsilon_{\phi,model}$ is related to the adopted subgrid closure while $\varepsilon_{\phi,num}$ contains aliasing errors as well as discretization errors. In case of proper dealiasing trough explicit filtering, $\varepsilon_{\phi,num}$ reduces exactly to the finite difference discretization errors.

In this work, the previous error decomposition is applied in two different ways. Following the work of Chow *et al.* [3], we first select the velocity field $u(x)$ as the variable of interest ϕ. The corresponding error spectrum and global error norm of the pointwise errors ε_u are then calculated as

$$E_\varepsilon(\kappa) = \widehat{\varepsilon_u}(\kappa)\,\widehat{\varepsilon_u}^*(-\kappa) \tag{34}$$

$$k_\varepsilon = \int_0^{\kappa_{max}} E_{\varepsilon_u}(\kappa)\, d\kappa \tag{35}$$

Remark that the global error norm k_ε corresponds to the L_2-norm, often used in error evaluation, by the relation $L_2 = 2\pi\sqrt{k_\varepsilon}$, and these errors always have a positive sign.

An alternative is to select the energy spectrum of the field $E_u(\kappa)$ for ϕ. The corresponding error definitions lead to the error between the energy spectra ε_E, and the total error on the global error norm $\varepsilon_{k,n}$

$$\varepsilon_E(\kappa) = \Delta E_u(\kappa) \tag{36}$$

$$\varepsilon_k = \int_0^{\kappa_{max}} \varepsilon_E(\kappa)\, d\kappa \tag{37}$$

suggested by Meyers *et al.* [11], differs from the previous method in the sense that the errors are evaluated in a statistical manner instead of a pointwise manner. Remark that the sign could be either positive or negative.

4.2. Results

The numerical error is given by the difference between the LES-solution with the pseudo-spectral method and the solution of the finite difference method. The energy spectra of these errors are given in Figure 3, at time step $t = 0.5$ before the shock is formed, and $t = 1.8$ after the shock is formed when the dissipation is at maximum. At $t = 0.5$

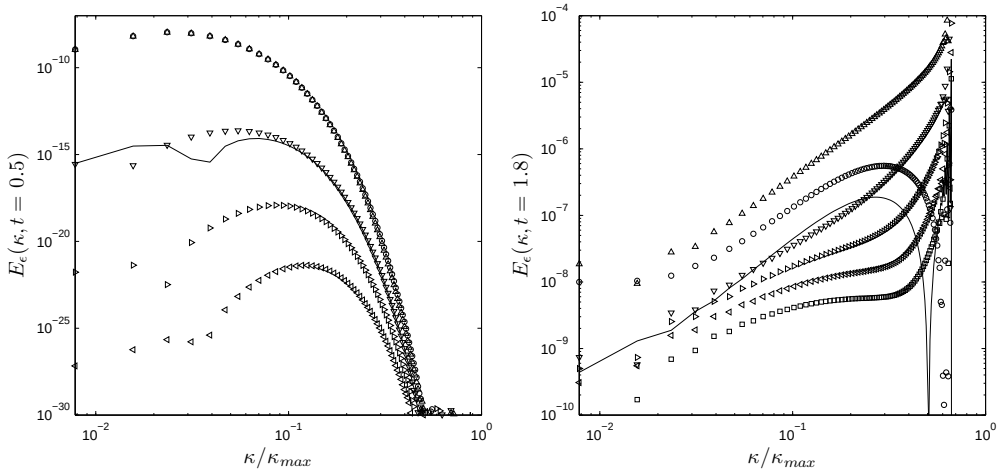

Figure 3: Error spectra E_ε on times $t = 0.5$ (left) and $t = 1.8$ (right): ($\triangle$) 2^{nd}-order central; ($\triangledown$) 4^{th}-order central; ($\triangleright$) 6^{th}-order central; ($\triangleleft$) 8^{th}-order central; ($\square$) 10^{th}-order central; ($\circ$) 2^{nd}-order DRP-scheme; (—) 2^{nd}-order dynamic scheme.

the dynamic coefficient is optimized only for the Fourier modes in the lower wavenumber range reaching 4^{th}-order asymptotic accuracy. At $t = 1.8$ the coefficient is optimized for the Fourier modes in the entire wavenumber range leading to a 2^{nd}-order asymptotic accurate optimized scheme, comparable to the DRP scheme, exceeding the accuracy of the higher-order schemes for $\frac{\kappa_c}{\kappa_{max}} \approx 0.4$. Although the results of the DRP scheme are similar to those of the dynamic scheme for a fully developed flow ($t = 1.8$), it tends only to 2^{nd}-order accuracy for the initial well-resolved flow e.g. at $t = 0.5$.

Figure 4 shows the global error norm k_ε and the error on the kinetic energy ε_k as function of time. It is observed from these figures that the dynamic scheme seamlessly adapts itself to the spectrum shape, reaching 4^{th}-order accuracy for $t < 1$, while reaching optimal accuracy for $t > 1$. Hence, for a fully developed shock wave the accuracy of the dynamic scheme exceeds the accuracy of the 8^{th}-order standard scheme. Although the DRP scheme does only have 2^{nd}-order accuracy for $t \leq 1$, it also reaches very high accuracy for $t > 1$. Notice that the dynamic scheme and the DRP scheme do not collapse for a fully developed spectrum. Both schemes are optimized for uniform spectrum shape. For the dispersion-relation preserving scheme, the coefficients themselves are determined a priori. For the dynamic scheme, only the blending factors f_1 and f_2 are determined a priori, whereas the dynamic coefficients $c^{dyn}_{k,n}$, $n = 1, 2$ are determined according to the spectral flow properties that scale with κ^{-2}.

5. Conclusions

We developed a *dynamic* low-dispersive finite difference scheme for Large-Eddy Simulation. The scheme is optimized dynamically during the simulation according to the spectral content of the flow and dispersion errors are minimized through the real-time adaption of the dynamic coefficients. In case of DNS resolution, the dynamic scheme reduces to the standard Taylor-based asymptotic 4^{th}-order finite difference scheme, whereas for LES resolution, the scheme seamlessly adapts to an optimized 2^{nd}-order finite difference scheme, comparable to 2^{nd}-order dispersion-relation preserving scheme of Tam *et al.* [7]. The results of the numerical test case agree very well with the theoretical predictions and indicate the large potential of the dynamic scheme.

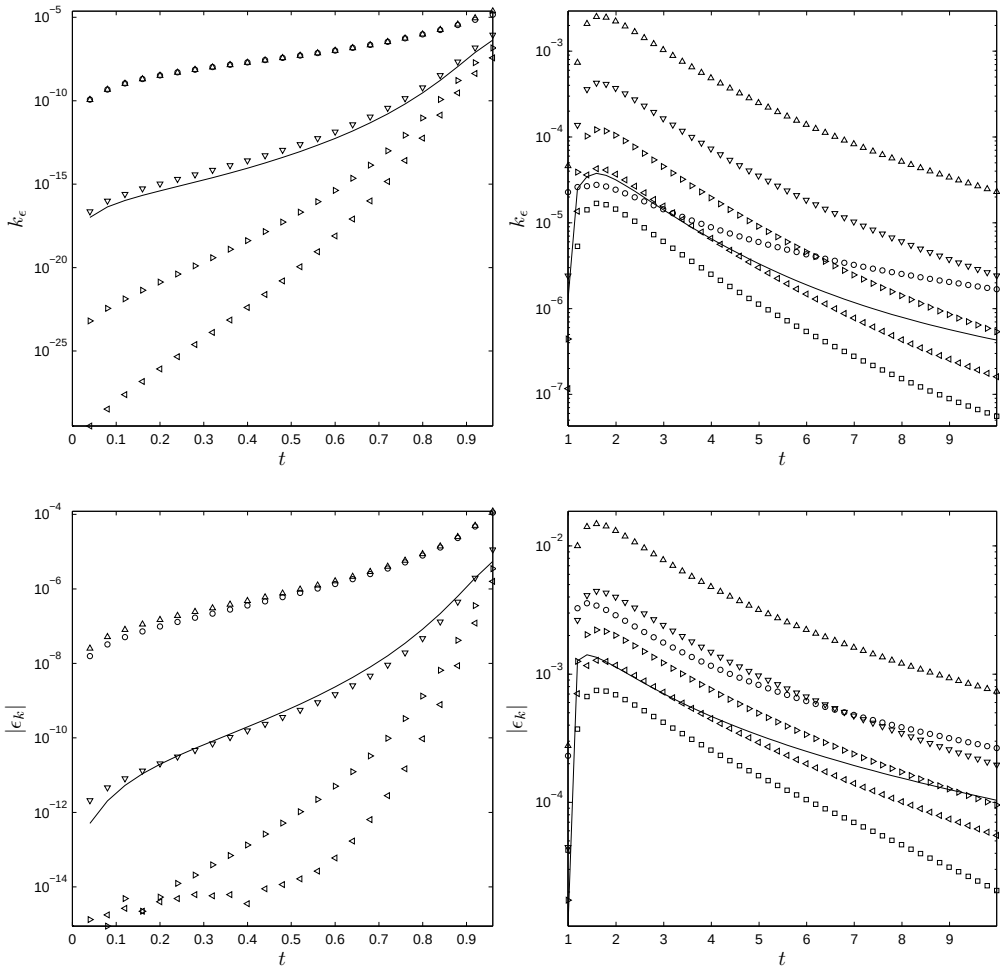

Figure 4: Global error norm k_ϵ (upper) and error on the kinetic energy ε_k (lower) as function of time. ($\triangle$) 2^{nd}-order central; ($\triangledown$) 4^{th}-order central; ($\triangleright$) 6^{th}-order central; ($\triangleleft$) 8^{th}-order central; ($\square$) 10^{th}-order central; ($\circ$) 2^{nd}-order DRP scheme; (—) 2^{nd}-order dynamic scheme.

References

[1] S. Ghosal. An analysis of numerical errors in large-eddy simulations of turbulence. *J. Comp. Phys.*, 125:187–206, January 1996.

[2] A. G. Kravchenko and P. Moin. On the effect of numerical errors in large-eddy simulations of turbulent flows. *J. Comp. Phys.*, 131:310–322, September 1997.

[3] F. K. Chow and P. Moin. A further study of numerical errors in large-eddy simulations. *J. Comp. Phys.*, 184:366–380, September 2003.

[4] S. A. Orszag. On the elimination of aliasing in finite-difference schemes by filtering high-wavenumber components. *Journal of the Atmospheric sciences*, 28:1074, April 1971.

[5] D. Fauconnier, C. De Langhe, and E. Dick. The dynamic procedure for accuracy improvement of numerical discretizations in fluid mechanics. *J. Comp. Phys.*, 224:1095–1123, 2007.

[6] Dieter Fauconnier, C. De Langhe, and E. Dick. The sampling-based dynamic procedure as tool for higher-order discretization. *Int. J. Num. Methods in Fluids*, 56:1241–1247, 2008.

[7] Christopher K. W. Tam and Jay C. Webb. Dispersion-relation-preserving finite difference schemes for computational acoustics. *J. Comp. Phys.*, 107:262–281, 1993.

[8] Arup Das and Robert. D. Moser. Optimal large-eddy simulation of forced burgers equation. *Phys. Fluids*, 14(12):4344–4351, 2002.

[9] Y. Morinishi, T. S. Lund, O. V. Vasilyev, and P. Moin. Fully conservative higher order finite difference schemes for incompressible flow. *J. Comput. Phys.*, 143(1):90–124, 1998.

[10] B. Vreman, B. Geurts, and H. Kuerten. Comparison of numerical schemes in large-eddy simulations of the temporal mixing layer. *Int. J. Num. Methods in Fluids*, 22:297–311, 1996.

[11] J. Meyers, B. Geurts, and M. Baelmans. Database analysis of errors in large-eddy simulation. *Phys. Fluids*, 15(9):2740–2755, September 2003.